

ADAPTIVE PROJECTED RESIDUAL NETWORKS FOR LEARNING PARAMETRIC MAPS FROM SPARSE DATA*

THOMAS O'LEARY-ROSEBERRY[†], XIAOSONG DU[‡], ANIRBAN CHAUDHURI[†],
JOAQUIM R. R. A. MARTINS[‡], KAREN WILLCOX[§], AND OMAR GHATTAS[¶]

Abstract.

We present a parsimonious surrogate framework for learning high dimensional parametric maps from limited training data. The need for parametric surrogates arises in many applications that require repeated queries of complex computational models. These applications include such “outer-loop” problems as Bayesian inverse problems, optimal experimental design, and optimal design and control under uncertainty, as well as real time inference and control problems. Many high dimensional parametric mappings admit low dimensional structure, which can be exploited by mapping-informed reduced bases of the inputs and outputs. Exploiting this property, we develop a framework for learning low dimensional approximations of such maps by adaptively constructing ResNet approximations between reduced bases of their inputs and output. Motivated by recent approximation theory for ResNets as discretizations of control flows, we prove a universal approximation property of our proposed adaptive projected ResNet framework, which motivates a related iterative algorithm for the ResNet construction. This strategy represents a confluence of the approximation theory and the algorithm since both make use of sequentially minimizing flows. In numerical examples we show that these parsimonious, mapping-informed architectures are able to achieve remarkably high accuracy given few training data, making them a desirable surrogate strategy to be implemented for minimal computational investment in training data generation.

1. Introduction. We seek to construct surrogates for parametric mappings, $m \mapsto q$, where $m \in \mathbb{R}^{d_M}$ are model parameters (input data) and $q \in \mathbb{R}^{d_Q}$ are quantities of interest (output data), which depend on inputs m , with probability distributions $\nu(m)$. The need for parametric surrogates arises in many problems in computational science, engineering, and machine learning. In a first class of problems, “outer-loop” problems, complex computational models need to be evaluated repeatedly for differing values of input parameters, making their solutions intractable if one is constrained to only use a high fidelity model. These “outer-loop” problems include uncertainty quantification, Bayesian inversion, Bayesian optimal experimental design, and optimization under uncertainty. Another class of problems requiring accurate surrogates is real-time decision making about complex systems; this includes early warning systems, and real-time inference.

We are specifically interested in settings arising from discretizations of physical models, however our proposed methodology can be applied to generic input–output data pairs. In the setting of discretized physical models (e.g. partial differential equations (PDEs)), inputs (and outputs) often represent approximations of infinite dimensional field quantities. Often \mathbb{R}^{d_M} represents a discretized approximation of

*This research was partially funded by the U.S. Department of Energy under ARPA-E award DE-AR0001208 and ASCR awards DE-SC0019303 and DE-SC0021239; and the U.S. Department of Defense under MURI award FA9550-21-1-0084.

[†]Oden Institute for Computational Engineering & Sciences, The University of Texas at Austin, Austin, TX (tom@oden.utexas.edu, anirban@oden.utexas.edu).

[‡]Department of Aerospace Engineering, University of Michigan (xsdu@umich.edu, jrram@umich.edu).

[§]Oden Institute for Computational Engineering & Sciences, Department of Aerospace Engineering and Engineering Mechanics, The University of Texas at Austin, Austin, TX (kwillcox@oden.utexas.edu).

[¶]Oden Institute for Computational Engineering & Sciences, Department of Mechanical Engineering, and Department of Geological Sciences, The University of Texas at Austin, Austin, TX (omar@oden.utexas.edu).

an infinite dimensional Banach space. The vector quantity of interest $q(m) \in \mathbb{R}^{d_Q}$ depends on m implicitly through a (typically nonlinear) state equation $R(u, m) = 0$, where the state variable u is an element of \mathbb{R}^{d_U} , another finite dimensional discretization of an infinite dimensional Banach space. Notably in this setting, the nominal discretization dimensions for the model d_M, d_Q may be much higher than the “information dimension” for the parametric mapping $m \mapsto q$. This key observation leads to the notion of bypassing the dependence on the discretization dimension by instead parametrizing the model in reduced bases of the inputs and outputs, which has been a successful strategy in scalable learning of parametric mappings [4, 38].

Outside of special cases where one can take advantage of analytical information about the functional form of $q(m)$, surrogates are typically constructed and trained via empirical risk minimization over training data $\{(m_i, q(m_i)) | m_i \sim \nu\}_{i=1}^N$. The question that we are concerned with can be stated: in settings where the use case of a parametric model is likely to amortize the costs of training data generation, what is the most information that we can extract from a given training dataset.

Our proposed methodology for this is to construct projected residual neural networks (ResNets) which learn low dimensional nonlinear mappings from a reduced basis for the input to a reduced basis for the output. The low dimensional residual neural networks we propose are constructed and trained adaptively, one layer at a time. This ResNet strategy allows us to construct surrogate models with the weight dimension independent of d_M, d_Q by making use of reduced bases. The adaptive training strategy is motivated by issues associated with neural network training, and empirically leads to better generalizability. Likewise the compressed ResNet layers allow one to start with a small amount of nonlinearity in a neural network and adapt this sequentially until significant overfitting is observed in the empirical risk minimization procedure. The strategy is highly scalable since it seeks to define neural network architectures that scale with the dimension of the information content of the map $m \mapsto q$, and not the nominal discretization dimension d_M, d_Q .

In order to motivate algorithms for the adaptive training and construction of the projected ResNet, we conceive of the ResNet as a time discretization of a limiting control flow. Recent approximation theory[21] shows that these flows are universal approximators of continuous functions on compact sets. Using this framework we prove that ResNet discretizations of control flows between reduced bases are universal approximators of L^2 integrable parametric functions on compact sets (i.e. there exists sufficient breadth, depth, to achieve a given accuracy). From an approximation theory standpoint this allows us to construct sequential minimizing flows that move input data to target data slowly via an ODE system. From a neural network training point of view this allows to motivate the sequential construction and training of these ResNet to realize better practical performance in realistic settings than dense feedforward networks of end-to-end trained ResNet.

In numerical experiments we consider two problems: one from parametric aerodynamic wing design optimization, and another from parametric PDE regression. In the former, no input dimension reduction is used since the inputs (flight constraints) are low dimensional, while the outputs are compressed. In the latter case both inputs and outputs are compressed, and derivative based dimension reduction is used to compress the inputs. Both experiments demonstrate that this general strategy can outperform typical neural network construction strategies in terms of generalization accuracy; these lean models can attain high generalizability for few training data, and can be adapted to increase representation power as more training data are available. In general this adaptive projected ResNet framework allows for an architectural strat-

egy that can be fine tuned to a specific problem: in terms of dimension reduction, nonlinearity, and learning “up to the noise”. Empirical results demonstrate that this strategy is robust to depth, breadth, and the availability of training data; while traditional neural networks may suffer due to too much depth, or too few training data, our proposed method performs reliably well.

1.1. Relevant work. A recent topic of interest in scientific machine learning is the deployment of neural networks as parametric surrogates [4, 6, 13, 20, 22, 24, 31, 32, 38]. Of particular relevance to this work are projection based parametric neural surrogates which seek to parametrize high dimensional maps by use of linear and nonlinear dimension reduction strategies [4, 6, 13, 31, 38].

The use of low rank residual network layers for non-spatial data has been proposed in various works before, but has not been widely adopted [33, 47]. Adaptive training of ResNets has been proposed in recent works [7, 11], and has performed well. Very relevant to the view of the neural networks as discretizations of ODEs are the following publications [8, 21, 41], which provide theoretical insight into the approximation capabilities of ResNets and relations with ODEs.

1.2. Contributions. The contributions of this work are both an approximation theoretic motivation of a class of projected ResNet models for parametric mappings, as well as practical algorithms for their construction. In Theorem 2.2 we posit the existence of a projected ResNet that can achieve arbitrarily good approximation of an $L^2(\mathbb{R}^{d_M}, \nu; \mathbb{R}^{d_Q})$ parametric function on a compact set $K \subset \mathbb{R}^{d_M}$. This view of the projected ResNet approximating function class motivates the algorithmic contribution of this work: construction of these approximating functions via time continuation / time discretization refinement via adaptive construction of the low dimensional ResNet parametrized between reduced bases of the inputs and the outputs.

2. Approximation by Projected ResNet. In this section, we motivate the use of projected ResNet architectures for approximating high dimensional parametric mappings in settings where limited training data are available. We do this by first reviewing input-output dimension reduced ridge functions, i.e. representing high dimensional maps by surrogates restricted to reduced bases of the inputs and outputs simultaneously. We then discuss the approximation of these dimension reduced ridge functions by ResNet. Approximation results are derived based on the connection between ResNet and discretization of control flow ODE systems, which under certain basic assumptions that many ResNet meet, are universal approximators of continuous functions on compact sets [21]. We extend this theory to derive a bound for the depth complexity of a ResNet approximation of a reduced basis mapping based on the desired accuracy, the size of the compact set, and the complexity of the associated approximating control flow. In this sense these projected ResNet can be thought of as “universal approximators” for parametric input-output maps.

2.1. Input–Output Reduced Ridge Functions. In this section we recount some theory regarding input-output projected ridge functions, which are discussed in [38], and based on results from [27, 39, 42, 48]. For a more detailed discussion, see [38]. Projected ridge functions are a means of exploiting low-dimensionality of an input-output map in architecting a parsimonious model. Projected ridge functions restrict the inputs and outputs of the map to reduced bases. Appropriately chosen reduced bases can embed key information of the map into the surrogate in order to make up for limited data in empirical risk minimization problems. These ridge functions are useful for analyzing representation power of the projected neural networks.

A ridge function is a composition of two functions $g \circ V_{r_M}$, where $V_{r_M} : \mathbb{R}^{d_M} \rightarrow \mathbb{R}^{r_M}$ is a linear mapping (a matrix in $\mathbb{R}^{r_M \times d_M}$), and $g : \mathbb{R}^{r_M} \rightarrow \mathbb{R}^{d_Q}$ is a measurable function. The ridge function mitigates the dependence of the input dimension d_M , by restricting the mapping to an r_M dimensional subspace of \mathbb{R}^{d_M} . The dependence of the output \mathbb{R}^{d_Q} can additionally be mitigated by employing a reduced basis for the output. In this case we modify the range of g to be \mathbb{R}^{r_Q} , and employ an affine transformation from \mathbb{R}^{r_Q} to \mathbb{R}^{d_Q} (a reduced basis $\Phi_{r_Q} \in \mathbb{R}^{d_Q \times r_Q}$, and an affine shift $b \in \mathbb{R}^{d_Q}$). The result is an input-output ridge function

$$(2.1) \quad q_r(m) = \Phi_{r_Q} g_r(V_{r_M}^T m) + b,$$

which mitigates high dimensional dependence (d_M, d_Q) linearly via reduced bases of dimensions (r_M, r_Q). Here $g_r : \mathbb{R}^{r_M} \rightarrow \mathbb{R}^{r_Q}$ is an input-output ridge function that learns a mapping between coefficients of the input basis and coefficient in the output basis. The nonlinearity of the mapping is approximated in a low dimensional mapping between \mathbb{R}^{r_M} and \mathbb{R}^{r_Q} .

Finding an appropriate ridge function q_r to approximate a given parametric map q involves several choices: the input reduced basis, the output reduced basis, and the choice for low dimensional functional approximation. Each decision depends on the choice of norm used to measure approximation errors. For our purposes we consider least-squares regression problems and the corresponding representation errors:

$$(2.2) \quad \mathbb{E}_\nu[\|q - q_r\|_{\ell^2(\mathbb{R}^{d_Q})}^2] = \int_{\mathbb{R}^{d_M}} \|q(m) - q_r(m)\|_{\ell^2(\mathbb{R}^{d_Q})}^2 d\nu(m),$$

which is the norm corresponding to the function space $L^2(\mathbb{R}^{d_M}, \nu; \mathbb{R}^{d_Q})$. We consider reduced bases that come from eigenbases of symmetric positive definite operators. Examples of these for input dimension reduction are Karhunen Loéve Expansion (KLE)[42] and active subspace (AS)[48], for the output proper orthogonal decomposition (POD)[27] is a canonical example. For each of these reduced bases, approximation errors can be bounded by trailing eigenvalues associated with these operators.

KLE exploits low dimensional structure for the input parameter distribution $\nu(m)$ by restricting the random variable m to the r_M dominant eigenvectors of the covariance matrix for ν , $C = V^{(KLE)} \text{diag}(c) (V^{(KLE)})^T$ where $(c_i, v_i)_{i \geq 1}$ are the eigenpairs in descending ordered by the eigenvalues c_i . KLE is useful in situations where the output uncertainty in q is inherited in a straightforward way from the input parameter distribution ν . AS exploits low dimensional geometric information about the map $m \mapsto q$ as revealed by the Jacobian of the map $\nabla q(m)$. active subspace builds a basis that takes into account both the sensitivity of the mapping, as well as the parameter uncertainty. This is done via construction of the eigenvalue basis for the following generalized eigenvalue problem

$$(2.3) \quad \mathbb{E}_\nu[\nabla q^T \nabla q] v_i = \lambda_i^{(AS)} C^{-1} v_i,$$

where $(\lambda_i^{(AS)}, v_i)_{i \geq 1}$ are the generalized eigenvalues sorted such that $\lambda_i \geq \lambda_j$ for $i < j$. In [48] bounds are established for ridge functions based on both KLE and AS. In both cases bounds are derived of the form:

$$(2.4) \quad \mathbb{E}_\nu \left[\|q - q_{r_M}\|_{\ell^2(\mathbb{R}^{d_Q})}^2 \right] \leq C_{\text{input}} \sum_{i=r_M+1}^{d_M} \lambda_i^{(\text{input})},$$

where q_{r_M} is a conditional expectation ridge function where the conditional expectation is taken with respect to the sigma-algebra generated by the input basis:

$$(2.5) \quad q_{r_M}(m) = \mathbb{E}_\nu[q|\sigma(V_{r_M}^{(\text{input})})](m).$$

These bounds establish that parametric mappings can be well-approximated by low dimensional ridge functions when there is significant decay in the eigenvalues $\lambda_i^{(\text{input})}$, and the prefactor constant C_{input} is not too large. In the case of KLE the constant $C_{\text{input}} = L_q^2$, and $\lambda_i^{(\text{input})} = c_i$. This bound takes into account the worst case amplifications of the map by making use of the Lipschitz constant of the map, L_q . In the case of AS, the constant $C_{\text{input}} = 1$ and $\lambda_i^{(\text{input})} = \lambda_i^{(\text{AS})}$. The AS bound does not involve worst case amplifications via a Lipschitz constant because the sensitivities of the map are taken directly into account via the construction of the input reduced basis. Indeed reduced basis neural networks using AS outperform identically architected reduced basis networks using KLE for parametric PDE regression problems [38]. The superior performance of the AS reduced basis comes at additional costs; these costs however require only marginally more (linear) computation than the nonlinear data generation when they are computed at training data locations. This can be done efficiently using adjoints [38], or sophisticated reverse-mode automatic differentiation when $d_M \gg d_Q$ [3].

For output reduced bases we consider POD, which is the eigenvector basis of the averaged outer product of the output: $\Phi \Lambda^Q \Phi^T = \mathbb{E}_\nu[qq^T]$, where $(\lambda_i^Q, \Phi_i)_{i \geq 1}$ are the generalized eigen-pairs. POD is the optimal rank r_Q linear basis for approximation of functions in $L^2(\mathbb{R}^{d_M}, \nu; \mathbb{R}^{d_Q})$, that is, it is the minimizer of

$$(2.6) \quad \min_{P_{r_M} \in \mathbb{R}^{d_M \times r_M}} \mathbb{E}_\nu \left[\|q - P_{r_M} P_{r_M}^T q\|_{\ell^2(\mathbb{R}^{d_Q})}^2 \right],$$

and the truncation error is given by $\mathbb{E}_\nu \left[\|q - \Phi_{r_Q} \Phi_{r_Q}^T q\|_{\ell^2(\mathbb{R}^{d_Q})}^2 \right] = \sum_{i=r_Q+1}^{d_Q} \lambda_i^Q$, see [27, 39]. Since we are concerned with approximations in a least-squares setting, POD is the optimal choice of reduced basis for the output. Combining these input and output reduced bases we can derive an approximation error for an input-output projected ridge function, which will guide our architectural choices for projected neural networks.

PROPOSITION 2.1 (Input–Output Ridge Function Error bound (Analogous to Proposition 2.2 in [38])). *Let $\nu(m) = \mathcal{N}(m, C)$ be a Gaussian distribution for the input parameter m , and the columns of $P_{r_M} \in \mathbb{R}^{d_M \times r_M}$ are a rank r_M reduced basis with an input such that the associated conditional expectation ridge function satisfies the truncation bound*

$$(2.7) \quad \mathbb{E}_\nu \left[\|q - q_{r_M}\|_{\ell^2(\mathbb{R}^{d_Q})}^2 \right] \leq C_{\text{input}} \sum_{i=r+1}^{d_M} \lambda_i^{(\text{input})}$$

for some $\lambda_i \geq \lambda_j \geq 0$. Define the rank r_Q POD decomposition for q_{r_M} as follows:

$$(2.8) \quad [\mathbb{E}_\nu[q_{r_M} q_{r_M}^T]]_{r_Q} = \hat{\Phi}_{r_Q} \hat{D}_{r_Q} \hat{\Phi}_{r_Q}^T.$$

Then the following bound holds for the input-output projected conditional expectation ridge function

$$(2.9) \quad \mathbb{E}_\nu \left[\|q - \hat{\Phi}_{r_Q} \hat{\Phi}_{r_Q}^T q_{r_M}\|_{\ell^2(\mathbb{R}^{d_Q})}^2 \right] \leq C_{\text{input}} \sum_{i=r+1}^{d_M} \lambda_i^{(\text{input})} + \sum_{i=r_Q+1}^{d_Q} (\lambda_i^Q).$$

The bound shows how the choices of input and output subspaces are interrelated, conceptually the first most important decision is the choice of input basis; one cannot well approximate a functional relationship if too many important parameters are thrown out. Both cases bound the approximation using POD decay of the conditional expectation ridge functions $q_{r_M}(m)$ instead of the output itself $q(m)$. The spectral convergence of the POD for q_{r_M} to POD for q can be seen by the following bound: let $\|q - q_{r_M}\|_2 = \|e\|_2 \leq \epsilon$,

$$\begin{aligned}
\|qq^T - q_{r_M}q_{r_M}^T\|_{\ell^2} &= \|qq^T - (q - e)(q - e)^T\|_2 \\
&= \|qe^T + eq^T - ee^T\|_2 \\
&\leq \|qe^T\|_2 + \|eq^T\|_2 + \|ee^T\|_2 \\
(2.10) \qquad \qquad \qquad &\leq 2L\epsilon + \epsilon^2.
\end{aligned}$$

The spectral bound $\mathbb{E}_\nu[\|qq^T - q_{r_M}q_{r_M}^T\|_2]$ holds due to the linearity of expectation. The error bounds in Proposition 2.1 establish that when the truncation errors in the input and output reduced representations decay rapidly, the parametric mapping can be well approximated by an input-output reduced conditional expectation ridge function on the joint reduced bases. The choice of ranks for the mapping are guided by the spectral decay of the operators associated with the construction of those bases. These bounds motivate the approximation of high dimensional maps by neural networks that are restricted to learn mappings between reduced subspaces of the inputs and outputs, such as in [4, 20, 38].

2.2. Control Flows and Projected ResNet. In this section we motivate the use of residual neural networks (ResNet) for the approximation of the low dimensional mapping between the input and output reduced bases. ResNet, among other types of neural networks are universal approximators for L^p measurable functions on compact sets [10, 16, 21, 23, 25]. We favor the use of ResNet over other networks principally due to their ability to be trained and constructed sequentially [7, 11], but also due to their potentially good approximation powers for sparse representation of the weights [23]. With projected ridge function surrogates as our target, we consider the approximation of functions $q_r : \mathbb{R}^r \rightarrow \mathbb{R}^r$. We take $r = r_M = r_Q$ for simplicity, and because we can require it to meet specific error tolerances (2.9). Additionally this dimension compatibility condition can be met via additional prolongation or restriction operators.

A residual neural network can be thought of as an Explicit Euler approximation of a control flow ODE (often referred to as neural ODEs) [8, 21, 41]. The control flow approximation temporally moves input data to output data, via appropriate choice of a right-hand-side for the ODE system

$$(2.11a) \qquad \qquad \qquad \frac{dz}{dt} = \phi(z, t)$$

$$(2.11b) \qquad \qquad \qquad z(0) = m_r = V_r^T m.$$

The goal is to find a right hand side ϕ , such that the generated flow moves arbitrary input data $m_r \in \mathbb{R}^r$ (view as initial conditions) approximately to the associated target output data $q_r \in \mathbb{R}^r$ in the eventual time limit $\lim_{t \rightarrow \infty} z(t) = q_r(m_r)$. Typically the form of the right hand side is

$$(2.12) \qquad \qquad \qquad \phi(z, t) = w_1(t)\sigma(t)(w_0(t)z + b(t))$$

where for each time t , $w_1(t) \in \mathbb{R}^{r \times k}$, $w_0(t) \in \mathbb{R}^{k \times r}$, $b \in \mathbb{R}^k$, where $k \leq r$ is a architecture parameter, and $\sigma(t)$ is a nonlinear function that is applied element-wise. When the dynamics are time integrated using Explicit Euler this system becomes a ResNet with l layers:

$$(2.13) \quad z_{k+1} = z_k + \Delta t w_{1k} \sigma_k(w_{0k} z_k + b_k),$$

where $\{(w_{1k}, w_{0k}, b_k)\}_{k=1}^l$ are the layer-wise coefficient arrays, and σ_k are the choices of activation functions. ResNet trained via empirical risk minimization can be thought of as approximations of control flows that move the sample input data to sample output data; the right hand sides are the process of a minimizing procedure attempting to control the approximation.

The representation capability of the control flow is related to the time horizon T , as well as the magnitude of right hand side of the control ODE. These two quantities together represent how “far” input data need to be moved to match output data, i.e. the quantity

$$(2.14) \quad \int_0^T \|w_1(t) \sigma(t)(w_0(t)z + b(t))\|_{\ell^2(\mathbb{R}^r)} dt.$$

The representation capability of the ResNet depends on the time horizon, the magnitude of the residual perturbation and additionally the time discretization parameter Δt . The representation capabilities of ResNet (and the connection to the representation powers of control flows) are related to the Barron function spaces, the elements of which can be represented to arbitrary accuracy by ReLU ResNet [12]. The Barron norm measures essentially how far data must be moved from inputs to outputs representation by a control flow, and is directly related to the time horizons and magnitude of right hand sides for control flow approximations. Note that ResNet naturally subsume the Δt discretization coefficients into the scaling of the layer weights, and therefore have the ability to dilate time. This makes it unclear how to specifically enforce a fine time discretization when constructing a ResNet. In order to constrain the flow to be smooth and “fine” in time discretization parameter, one can impose constraints on the norm of each layers perturbation. However since the approximation power of the ResNet is ultimately related to how far the control flow moves points, (equation (2.14)), restrictions on layer perturbations then require many layers. This is consistent with the asymptotic approximation of the control flow: in the limit as $\Delta t \rightarrow 0$, each layers contributions converge uniformly to zero, and the required depth $\rightarrow \infty$.

In [21], the authors show that a sufficient condition for the class of functional approximations by generating flows (2.11) to be universal approximators of continuous functions on compact sets is that functional representation of the right hand side for the ODE satisfies two conditions that are both highly relevant to ResNet. The first condition is a restricted affine invariance property (the function space is closed under affine operations). The second condition is that the closure of the class contains a “well-function”. A well-function is a function for which the function’s nullspace contains an open bounded set. This property makes it so that the update in the neural ODE (2.11) can leave entire regions of \mathbb{R}^r unchanged while modifying other certain portions. This allows for the general construction of control flows that work on moving local regions of the input to their targets in the output, and thus universal approximation of continuous functions on compact set. For example, ReLU is a well-function because it maps the entire left half-plane to zero. Many other popular activation functions in machine learning are well-functions. The universal approximation result in

[21] states that there exists a finite time ($T > 0$) control flow that can get arbitrarily close to approximating any continuous function on a compact set $K \subset \mathbb{R}^r$. We now state a representation error bound for input-output projected ResNet approximations of parametric mappings. Without loss of generality we consider zero-mean mappings $m \mapsto q$, since we can always subtract the mean from the map (or equivalently have the mean be the last layer bias in the output representation).

THEOREM 2.2. *Representation Error Bound for Reduced Basis ResNet* Given a parametric mapping $q \in L^2(\mathbb{R}^{d_M}, \nu; \mathbb{R}^{d_Q})$, that can be approximated by restriction to rank $r < \{d_M, d_Q\}$ reduced bases of the inputs with truncation error given by:

$$(2.15) \quad \mathbb{E}_\nu \left[\|q(m) - \hat{\Phi}_r q_r(V_r^T m)\|_{\ell^2(\mathbb{R}^{d_Q})} \right] \leq \zeta_r$$

Where $q_r : \mathbb{R}^r \rightarrow \mathbb{R}^r$ is a ridge function that approximates q between the reduced basis for the inputs V_r and the orthonormal reduced basis for the output Φ_r . Then for any compact set $K \subset \mathbb{R}^{d_M}$ there exists an input-output projected ResNet $f_r(V_r^T m, w)$ such that

$$(2.16) \quad \int_{K \subset \mathbb{R}^{d_M}} \|q(m) - \hat{\Phi}_r f_r(V_r^T m, w)\|_{\ell^2(\mathbb{R}^{d_Q})} d\nu(m) \leq 2\zeta_r,$$

and the depth of the ResNet is $O\left(\frac{Te^T|K|}{\zeta_r}\right)$, where T is the time horizon for the associated control flow mapping that is the continuous time analogue of the ResNet.

See Appendix A for proof. Additionally noted in the appendix, are conditions under which the depth complexity can be reduced to $O\left(\frac{T|K|}{\epsilon}\right)$, which is related to details of the construction of the control flow being approximated via Explicit Euler.

Since the truncation errors can be made arbitrarily small by the choice of rank for the basis, this result establishes that high dimensional parametric mappings restricted to compact sets can be approximately arbitrarily well by projected ResNet, and establishes an approximation bound that depends on the truncation error as a result of the projections, as well as the complexity in the ResNet approximation of the reduced ridge function. In particular when the high dimensional map can be well-approximated for $r \ll \{d_M, d_Q\}$ the weight complexity of the ResNet can be reduced significantly compared to overparametrized networks. As the result states, the ResNet depth is inversely proportional to the desired accuracy, and proportional to the size of the desired region where the map is to be approximated $|K|$, as well as a complexity upper bound for the approximation of the restricted nonlinear map via a control flow with time horizon T . Inner regular measures can be approximated arbitrarily well on compact sets; that is, for any $\epsilon > 0$, there exists a compact set K_ϵ such that the measure of K_ϵ^c is bounded by ϵ . This makes the result sufficiently general, however extending this result to all of \mathbb{R}^{d_M} is tricky since the depth complexity for the ResNet is a function of $|K_\epsilon|$. More sophisticated bounds could make use of results in concentration of measure in order to mitigate the dependence on $|K|$.

The result hinges on the existence of a finite time horizon approximating control flow for the target function. Unfortunately the result does not say anything generally about how large T is as a function of the complexity of the target function q_r . In the case of 1D-monotonic functions a bound is given in [21] in terms of the regularity of the target function; when the total variation of the Jacobian of the map is smaller, less time is needed to move the input data space to the output data space. In future

academic work, hopefully these approximation rates can be extended to high dimensional non-monotonic functions; one would expect that smoother functions are easier to approximate.

2.3. Balancing the various errors. The result in Theorem 2.2 gives an approximation bound for the representation capabilities of ResNet in representing parametric maps. Two major hurdles remain for realizing such approximations in practice: the first is the approximation of the stochastic integral via Monte Carlo samples $\{(m_i, q(m_i)) | m_i \sim \nu\}_{i=1}^{N_{\text{data}}}$, and the second is the nonconvex empirical risk minimization problem for training the neural network. The approximation of the stochastic integral via Monte Carlo will be a fundamental limitation in practice for many parametric mappings, since the dominant costs will almost always be associated with the generation of training data, and not the construction and training of neural networks. In dealing with this issue we seek to *balance* the different approximation errors. The approximating neural network is not directly learning the true parametric mapping, but instead instances of the mapping on finite training data. Defining $\text{misfit}(m_i) = \|q(m_i) - \hat{\Phi}_r f_r(V_r^T m_i, w)\|_{\ell^2(\mathbb{R}^{d_Q})}$, we can include the Monte Carlo error in the representation via the triangle inequality:

$$(2.17) \quad \int_{K \subset \mathbb{C}^{\mathbb{R}^{d_M}}} \|q(m) - \hat{\Phi}_r f_r(V_r^T m, w)\|_{\ell^2(\mathbb{R}^{d_Q})} d\nu(m) \leq$$

$$\underbrace{\zeta_r}_{\text{truncation error}} + \underbrace{\zeta_r}_{\text{ResNet error}} + \underbrace{\frac{\text{std}_\nu(\text{misfit})}{\sqrt{N_{\text{train}}}}}_{\text{Monte Carlo error}}.$$

In order to achieve arbitrary accuracy we need all three of these errors to tend to zero uniformly. In the pre-asymptotic regime we strive for the errors to be balanced. The fundamental representation limitation becomes the availability of training data, so we seek to balance the representation errors (Theorem 2.2) specifically to the Monte Carlo errors (the level of the noise). If the noise level is lower than the representation power, then we have left generalization accuracy on the table. If the noise level is significantly higher than the representation capability, then we risk learning stochastic fluctuations in the training data that are not relevant to the true parametric mapping (i.e. overfitting).

In practice the projection errors are likely the easiest to control since they can be estimated easily via approximation of trailing eigenvalues using randomized methods [28]. For subspaces such as AS, KLE and POD where the approximation errors can be estimated directly, we can decide upon a proper choice of r via inspection of the spectral decay of the associated operators, this dimension is associated with the “intrinsic dimensionality” of the parametric map. The most difficult error to control is the ResNet error due to its association with a nonconvex optimization problem. In what follows we motivate a practical algorithm for adaptive construction and training of these ResNet that attempts to ease the nonconvexity of the associated empirical risk minimization training problem.

3. Adaptive Construction and Training of Projected ResNet. Deep neural network training is notoriously difficult; deeper networks have greater representation power, but their practical performance hinges on the availability of training data; many strategies in deep learning such as overparametrization require large amounts of training data for their success. Motivated by achieving good generalizability for limited training data, we propose an adaptive training and construction strategy, to

sequentially add layers to a ResNet up to the noise-level of the training data. This strategy combines the construction of the ResNet and the training into one combined iterative process. Unlike much of deep learning, this strategy represents a confluence between both the approximation theory as well as the training, since in this case both make use of sequentially minimizing approximating flows.

The strategy allows a tractable path to constructing a deep network (with high approximation power), while also mitigating issues associated with the associated training problem in the few-data regime. Note that other neural networks such as dense feedforward cannot be constructed and trained in this way since additional non-linear compositions will distort the previous approximation significantly; only ResNet like architectures can be built and trained in this fashion.

In the first offline step the user can choose an appropriate set of reduced basis for the inputs and outputs, without loss of generality take $r = r_M = r_Q \ll \{d_M, d_Q\}$ ¹. Truncation strategies using AS, KLE and POD allow us to decide the dimension of the reduced basis based on spectral decay of operators associated with the construction of these bases. So for these bases the proper dimensionality can be inferred ahead of time, or based on a user defined tolerance such as spectral decay rate or randomized error estimators. What is left is the architectural decisions of the ResNet. Since we seek a parsimonious representation of the mapping that representation power is tied to what can be learned from a sparse dataset, we use a sparse representation for the ResNet layer where the matrices $w_{1k} \in \mathbb{R}_{r \times r_k}$, $w_{0k} \in \mathbb{R}^{r_k \times r}$ are low rank ($r_k < r$) [33]. The algorithm then constructs a residual network one layer at a time by adding a low rank projected residual network unit:

$$(3.1) \quad z_{k+1} = z_k + w_{1k}\sigma(w_{0k}z_k + b_k).$$

For small $\|w_{1k}\sigma(w_{0k}z_k + b_k)\|$, layer $k+1$ represents a small nonlinear perturbation of the representation of the map. The layer can either be trained separately, or in combination with the prior layers. The former builds a flow where future times are conditioned on previous times via minimization of a loss function. The latter seeks to build a long discretized flow via temporal refinement. Training one layer at a time has the benefit of solving a sequence of simple optimization problems. Training all at once has the added benefit of superior representation capability. As an heuristic for the imbalance of the representation power and stochasticity of the data, one can determine the termination of the iterative construction of the ResNet via depth by monitoring discrepancies between training accuracy and validation accuracy.

In order to avoid overfitting we propose using a small number of optimization iterations for each sequential training and then have one additional end-to-end training once the terminal depth is found. Based on experimentation we have found that stochastic gradient based methods are good for the individual layer trainings during construction from initial guesses, the termination of this process serves as a good initial guess for the final end-to-end training, for which second order methods perform well [35, 36] in extracting extra generalization accuracy from a good initial guess (e.g. transfer learning). We summarize the adaptive training algorithm below.

¹Otherwise one can add an upsampling or downsampling layer to the beginning or end of the network to enforce dimensional compatibility for the ResNet layer.

Algorithm 3.1 Adaptive construction of Projected ResNet

- 1: Given reduced bases for inputs and outputs: V_r, Φ_r
 - 2: $z_0(m) = V_r^T m$ (truncated representation of input data)
 - 3: $k = 0$
 - 4: **while** Validation accuracy is increasing **do**
 - 5: Train Projected ResNet $f(m) = \Phi_r z_{k+1}(m) + b_Q$,
 - 6: where $z_{k+1}(m) = z_k(m) + w_{k+1,2}\sigma(w_{k+1,1}z_k(m) + b_{k+1})$
 - 7: $k = k + 1$
 - 8: **end while**
 - 9: One final end to end training (using second order optimizer)
 - 10: **return** Projected ResNet
-

The analysis and algorithmic framework are easily adaptable to any setting where an input-output map needs to be learned from data, and a reduced basis methodology is appropriate for either the input or output representation spaces, or both. In the parametric PDE setting it is useful to do dimension reduction on both inputs and outputs.

4. Numerical Experiments. In this section we demonstrate the benefits of adaptively constructed projected ResNet for two tasks: inverse aerodynamic shape design and parametric PDE inference. We study the accuracy of the network as a function of the truncation dimension r , the depth, and the amount of data available during training. We compare against different dense neural network strategies as in [38], where the number of hidden layers is determined by the output dimension d_Q , or the truncation dimension of the projected network r . The former we refer to as a “full dense”, and the latter “truncated dense”. We also compare against the same ResNet architecture trained end-to-end (without the adaptive procedure); these strategies represent baselines for these regression tasks. In all cases we compare all of the architectural strategies for fixed total number of optimization epochs (the sum total of each epoch used in the adaptive trainings), with access to the exact same data and same optimizers. This does not take into account that the computational costs of optimization for the low dimensional models are much lower; that is an added bonus.

In this work we use Adam optimizer with default settings for the step size and momentum parameters. This is to avoid specific hyperparameter tuning that makes the work less general. For the first set of results we only use Adam since the problem is low dimensional. For the higher dimensional second set of numerical results we use a combination of Adam and Low Rank Saddle Free Newton (LRSFN), due to its ability to improve upon the performance of first order optimizers given a good guess [36, 36]. We note that we do not compare against projected dense strategies as in [38], since in that work, an inexact Newton CG optimizer was required to achieve suitable accuracy. In experiments, projected dense networks were unable to attain suitable generalization accuracies when using Adam. One of the major selling points of the projected ResNet over the projected dense strategy, beyond adaptability, is robustness to the choice of the optimizer. Code for the parametric PDE surrogates is in the `hippyflow` library [37] which builds on the `hippylib` library[45], which implements scalable adjoint-based methods for PDE-based inverse problems using `FEniCS`[2]. Code for the LRSFN optimizer can be found in the `hessianlearn` library[34], a library for Hessian based stochastic optimization in `TensorFlow` [1].

4.1. Inverse Aerodynamic Shape Optimization. In this section, we detail the aerodynamic wing design problem setup formulated by the Aerodynamic Design Optimization Discussion Group (ADODG) of the American Institute of Aeronautics and Astronautics (AIAA). The AIAA ADODG formulates a series of benchmark cases which provide a foundation for rational assessment of the multitudinous aerodynamic design optimization approaches to problems of interest. In particular, we generalize the ADODG Case 3, *i.e.*, drag minimization of a rectangular wing in inviscid subsonic lifting flow, in the following ways: we generalize the inviscid flow to viscous flow which is a more challenging test case and requires to solve the Reynolds-averaged Navier–Stokes (RANS) equations; we incorporate free-form deformation (FFD) control points as design variables besides a twist angle distribution. We expand each of the flight conditions and design requirements from a single value to a uniform parameter distribution $\nu(m)$ delineated in Table 1, this then defines our task for parametric regression; the mapping from design constraints m to drag-optimal geometry $q(m)$. Additional details about the software, and data used in this application can be found in Appendix B.

4.1.1. Problem Description. We set up the inverse aerodynamic design problem by following the ADODG Case 3, drag minimization of a rectangular wing 1 with the NACA 0012 airfoil as the wing section in inviscid subsonic flow. For the purpose of testing the proposed algorithm in practical and challenging applications, we consider viscous flow by solving the RANS equations. We consider 200 FFD control points to parameterize the wing geometry, with each of 10 wing sections has 10 FFD control points on the upper surface and 10 on the lower surface 2. Plus, we use 10 twist variables which are evenly distributed along the z axis (span-wise direction) within the range of $[0.0, 3.0]$. The angle of attack is used as a dummy variable to satisfy the target lift coefficient constraint. In this section we focus in regression for the FFD control points only, since these data share geometric similarity the POD basis admits low rank structure. Learning the twist and angle of attack are very low dimensional and do not lend themselves well to dimension reduction; shallow dense is sufficient for that task. Since the flight condition is at low speed, varying Mach number will not significantly affect the aerodynamic performance. Therefore, we extend the other design requirements for the demonstration purpose of the proposed algorithm. We set the target lift coefficient within the range of $[0.2, 0.4]$, vary the lower bound of moment coefficient by $\pm 20\%$ to make a range of $[-0.11, -0.074]$, set the lower bound of internal volume as $0.8 \sim 1.0$ with respect to the baseline, and arrange Reynolds number with the range of $[1 \times 10^5, 1 \times 10^7]$. We summarize the wing design problem below in Table 1.

4.1.2. Results. In this aerodynamic wing design problem the input dimension is small so we do not use any input dimension reduction. Instead we only reduce the 200 dimensional output, using POD. Thus the truncation errors in the analysis only apply to the output representation. For these numerical results we use a 10 dimensional POD basis for the output representation. As a first step in the projected ResNet we prolongate the 4 dimensional data to the 10 dimensional representation via using a dense matrix. The ResNet then learns the mapping between the prolonged input data representation and the 10-dimensional output basis for POD. For each layer of the projected ResNet we use rank 4.

We compare the adaptive projected ResNet strategy (AR) with an end-to-end trained identical projected ResNet (ER). We compare these two strategies to a truncated dense (TD) strategy that has hidden layer dimensions that are the same as the

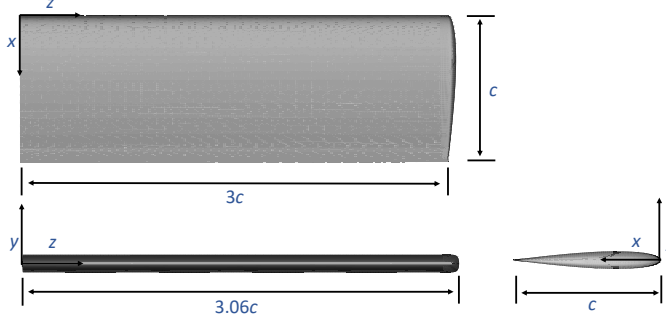
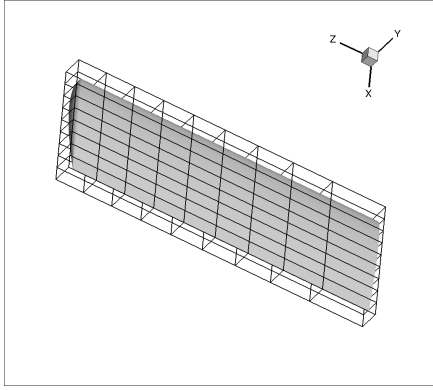
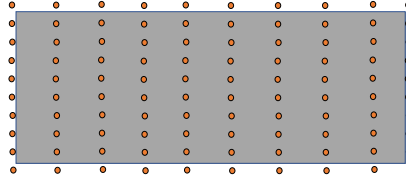


Fig. 1: The rectangular wing has a chord of $c = 1$, half wingspan of $3c$, a wing-tip cap of $0.06c$, and no twist angle, dihedral angle or sweep angle.



(a) FFD box used for optimization.



(b) FFD control points.

Fig. 2: A total of 200 (10 sections \times 20 FFD control points / section) geometric variables provide sufficient design flexibility.

POD basis rank, as well as a full space dense (FD) overparametrized strategy, where the hidden layer dimensions are the same as the output dimension (200). We study the effects of availability of training data, and the depth of the neural networks. All networks use the same inner layer activation function (softplus). We compare the effects of amount of training data, and repeat runs over 20 different independent shufflings of a larger dataset. We define generalization accuracy with respect to the $\ell^1(\mathbb{R}^{d_Q})$ norm, which is a common choice for aerodynamic shape optimization problems.

$$(4.1) \quad \ell^1 \text{ Accuracy} = \mathbb{E}_\nu \left[1 - \frac{\|q - f\|_{\ell^1(\mathbb{R}^{d_Q})}}{\|q\|_{\ell^1(\mathbb{R}^{d_Q})}} \right]$$

In order to emphasize the relative strengths of each network architecture with limited training data we run the trainings for 40 different instances of training data. We report median generalization accuracies $\pm 30\%$, as well as the maximum accuracies in some cases. We begin by studying a comparison of the different networks for the

Table 1: 3D wing optimization problem formulation.

	Function or variable	Description	Quantity
minimize	C_D	Drag coefficient	
w.r.t.	\mathbf{x}	FFD control points	200
	$\boldsymbol{\lambda}$	Twist angle	9
	α	Angle of attack	1
	Total design variables		210
subject to	$C_L^* = 0.2625$	Lift-coefficient constraint	1
	$C_M > -0.092$	Moment-coefficient constraint	1
	$0.8V_0 \leq V \leq 1.5V_0$	Internal volume constraint	1
	$0.8\mathbf{t}_{\text{base}} \leq \mathbf{t} \leq 1.5\mathbf{t}_{\text{base}}$	Thickness constraints	100
	Total constraints		103
Conditions	$M = 0.5$	Mach number	
	$Re = 1 \times 10^6$	Reynolds number	

depth 5 case.

In Figure 3 we see that the adaptive ResNet strategy outperforms the dense strategies in the low data limit, however the full space dense network is able to perform about as well once around 100 data become available. The truncated dense networks and end-to-end ResNet perform worse; as will become apparent in further results, the adaptive training routine consistently outperforms the end-to-end training.

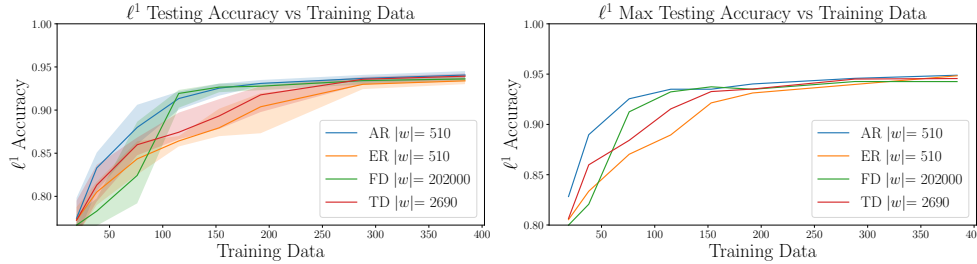


Fig. 3: Depth 5 Comparison of Networks

Figure 4 shows similar results as we double the depth to 10. Again the adaptive ResNet outperforms all of the other models. As the depth increases the dense networks get harder to train, and the end-to-end ResNet tends to perform better.

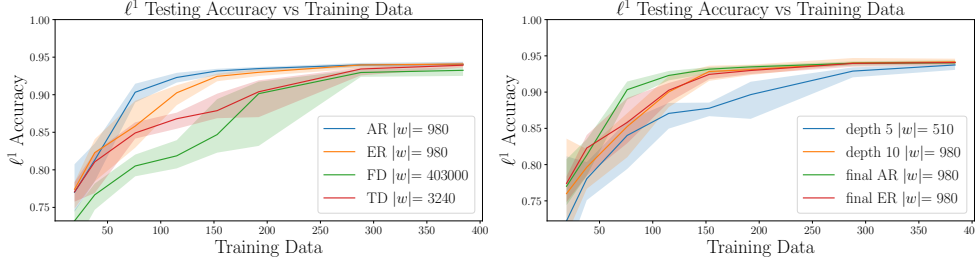


Fig. 4: Depth 10 Comparison of Networks

Figure 5 shows the degradation of performance for the dense networks as more depth is added, while the performance of the ResNet is about the same. This shows that adding additional depth may not add much once the informed modes in the data are well represented, but that the ResNet strategy is a much safer way to add depth than using dense feedforward networks for parametric inference.

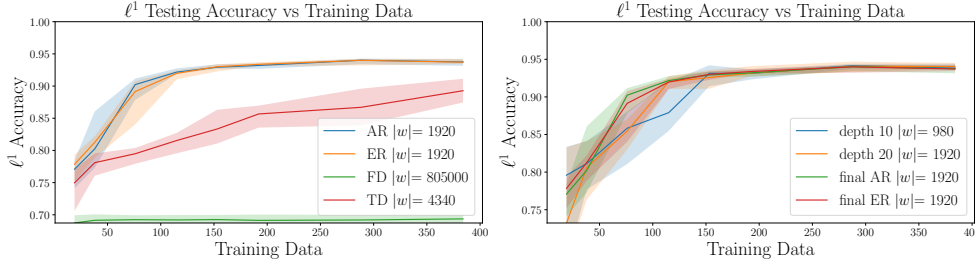


Fig. 5: Depth 10 Comparison of Networks

These numerical results show that the adaptive ResNet strategy can outperform other conventional black-box neural network strategies, when limited data are available, and additionally show that they do not suffer from the degraded performance adding more depth like dense feedforward networks. In the next example which has high dimensional inputs and outputs, we can see more significant improvements over baseline networks.

4.2. Parametric Helmholtz Regression. For our last numerical example, we consider parametric Helmholtz regression. Accurate surrogates for PDE parameter-to-observable mappings can be used to make tractable the solution of high dimensional inference and optimization problems, such as Bayesian inference, and optimal experimental design. We consider a 2D Helmholtz parameter to observable problem similar to that of [38]. The parameter shows up nonlinearly as a log-prefactor of the

wavenumber k . The parameter to observable map is formulated as follows.

$$\begin{aligned}
(4.2a) \quad & -\Delta u - (ke^m)^2 u = f \quad \text{in } \Omega \\
(4.2b) \quad & \text{PML boundary condition on } \partial\Omega \setminus \Gamma_{\text{top}} \\
(4.2c) \quad & \nabla u \cdot n = 0 \text{ on } \Gamma_{\text{top}} \\
(4.2d) \quad & q(m) = Bu(m) = [u(\mathbf{x}^{(i)}, m)] \quad \text{at } \mathbf{x}^{(i)} \in \Omega \\
(4.2e) \quad & \Omega = (0, 3)^2.
\end{aligned}$$

The random parameter m is sampled from a Matérn Gaussian distribution with zero mean and covariance given by the inverse of an elliptic PDE operator: $C = (I - 5.0\nabla \cdot (\Theta \nabla))^{-2}$. The matrix $\Theta \in \mathbb{R}^{2 \times 2}$ introduces spatial anisotropy to the random field. The mesh used for this problem is 128×128 , and the model parameter m is represented by linear finite elements, making the input dimension $16,641 = (129)^2$. The problem has 100 observation points of a 2D wave field so the output dimension is 200. The perfectly matched layer (PML) boundary conditions on the side and bottom of the domain allow us to simulate a semi-infinite domain [9]; only the top surface can reflect the waves. The right hand side contains a single source point located at $(0.775, 2.85)$, and the observation points are located in a grid in $(0.575, 0.975) \times (2.75, 2.95)$; none of the observations take place at the source. The wave number for this problem is 9.118. This is a notoriously difficult problem due to the highly oscillatory nature of the wavefield solution of Helmholtz, as well as the nonlinear dependence on the model parameter m . The problem is highly relevant to inference and optimization problems related to imaging, and subsurface modeling.

As with the last example we compare with truncated dense networks using the same breadth as the projected ResNet, and full-space dense network which has hidden layer dimensions of 200. In this case we also compare against identically architected projected ResNet, which use active subspace and Karhunen-Loève Expansion for the input dimension reduction. For output dimension reduction we employ POD in all cases. Projected networks using active subspace are referred to as derivative informed projected networks (DIPNet) [38], in this case we refer to the ResNet version as DIPResNet, and the KLE analogue as KLEResNet. As with the last example we use layer ranks of 4 for the ResNet, and use softplus activation for all of the nonlinear layers. In this example we use the normalized ℓ^2 accuracy to compare the different network strategies:

$$(4.3) \quad \ell^2 \text{ Accuracy} = \mathbb{E}_\nu \left[1 - \frac{\|q - f\|_{\ell^2(\mathbb{R}^{d_Q})}}{\|q\|_{\ell^2(\mathbb{R}^{d_Q})}} \right].$$

We compare the different strategies as a function of the amount of training data seen, as well as the depth. For this case we set aside 512 data for testing accuracy. Additionally validation data that are 25% the size of the training data are used for validation accuracy during the adaptive training of the ResNet. As was noted before we train the networks using Adam as they are being constructed, and then perform an additional last optimization using LRSFN, which increases the generalization accuracy; for a discussion of numerical results that provide empirical justification of this strategy, see the Appendix.

We begin by considering a case of depth 5, starting with breadth $r = 32$ and increasing it to enrich the basis function representation. Figure 6 shows comparisons of the ResNet with the other dense models. The left part of Figure 6 shows

that the adaptively trained DIPResNet outperformed all other models until the overparametrized full dense model begin outperforming the breadth 32 depth 5 adaptively trained DIPResNet around 1500 training data; this is an expected result in machine learning, that overparametrized networks *should* win in the high data limit (note however that the full dense strategy is not scalable and will suffer with mesh refinement, see [38]). The right plot compares the performance of the DIPResNet (which used active subspace basis) vs KLEResNet. This plot shows that while the two architectures initially have similar performance characteristics in the extremely low training data limit, the DIPResNet significantly outperforms the KLEResNet as more training data become available. Additionally though, the adaptive KLEResNet outperforms the end-to-end trained DIPResNet until about 4,250 training data are available. This plot demonstrates that *both* the map informed reduced basis (AS) and the adaptive training strategy help improve accuracy when few training data are available.

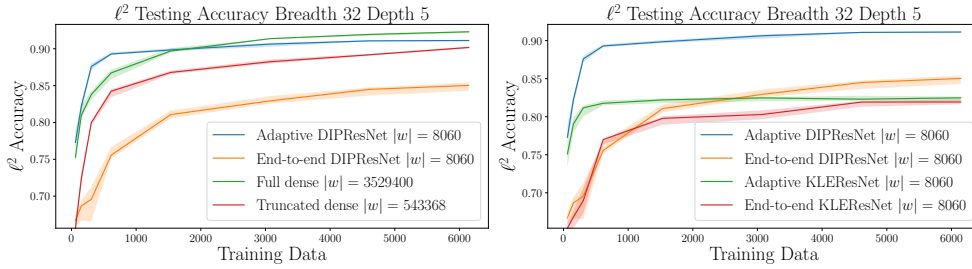


Fig. 6: Depth 5 Breadth 32 Comparison of Networks

Since the Helmholtz problem is highly oscillatory it would make sense that we would need larger reduced basis representations to faithfully capture these higher order effects. Figures 7 and 8 demonstrate the effects of enriching both the input and output basis representations (as well as increasing the intermediate hidden neuron representations in the truncated dense network), the only constant between all of these figures is the full dense network. As more basis functions are added to the inputs and outputs the adaptively trained DIPResNet reliably outperforms the overparametrized fully dense network. The effects of increasing the breadth are to shift the accuracy curves up, as one might expect. Note that due to convergence issues the full dense is undefined for training data less than 500, this effect demonstrates the robustness of the ResNet architecture to optimizer issues.

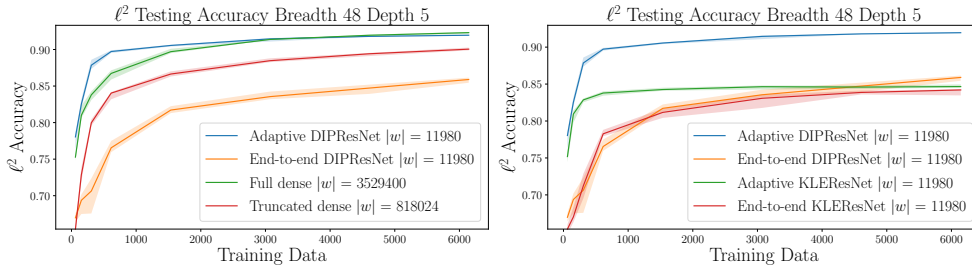


Fig. 7: Depth 5 Breadth 48 Comparison of Networks

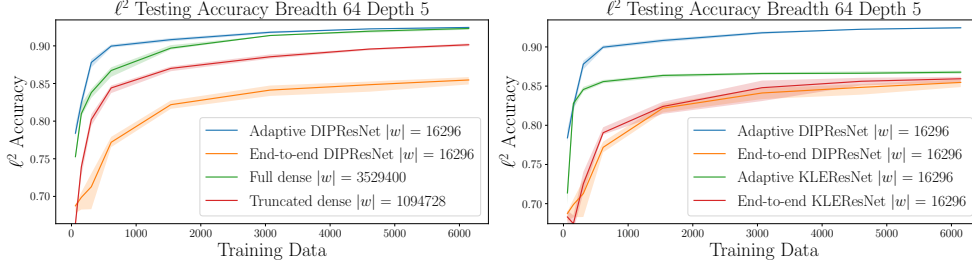


Fig. 8: Depth 5 Breadth 64 Comparison of Networks

In the next set of numerical experiments, we study the effects of increasing the depth of the networks, in particular we are interested in robustness of the architectural strategies to added depth. Below in Figures 9 and 10 we can see the ResNet strategies are robust to adding more depth, while the full generic network tends to suffer. Interestingly the end-to-end trained ResNet are able to perform better as more depth is added, but the dense networks are not.

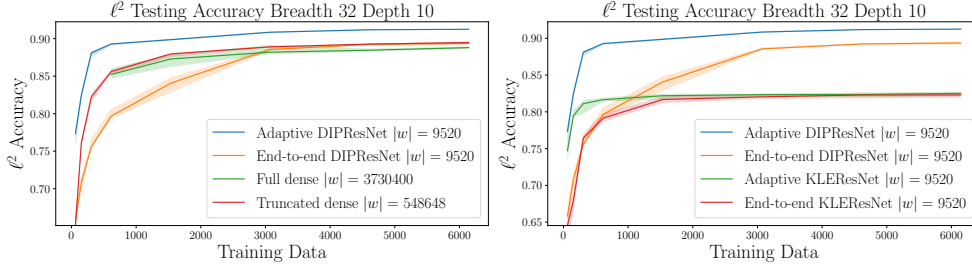


Fig. 9: Depth 10 Breadth 32 Comparison of Networks

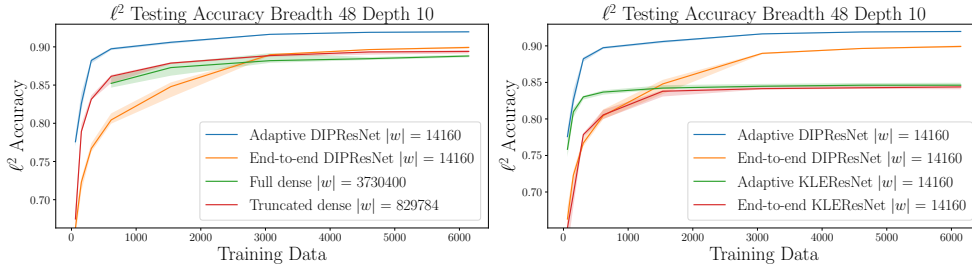


Fig. 10: Depth 10 Breadth 48 Comparison of Networks

The issues with overparametrization can be seen acutely in Figure 11, where as more depth is added the ResNet strategies (both adaptive and one-shot training) consistently maintain accuracy, while the dense strategies performance is significantly deteriorated. This plot suggests that the projected ResNet architectures are less susceptible to the depth “peaking phenomenon” [17], where for fixed training data,

the accuracy of a network improves initially as depth is added, but eventually the performance begins to deteriorate. Note that in all cases the training error reaches zero, so this suggests that the projected neural networks may be better suited to maintaining generalization accuracy, in comparison to the other dense strategies.

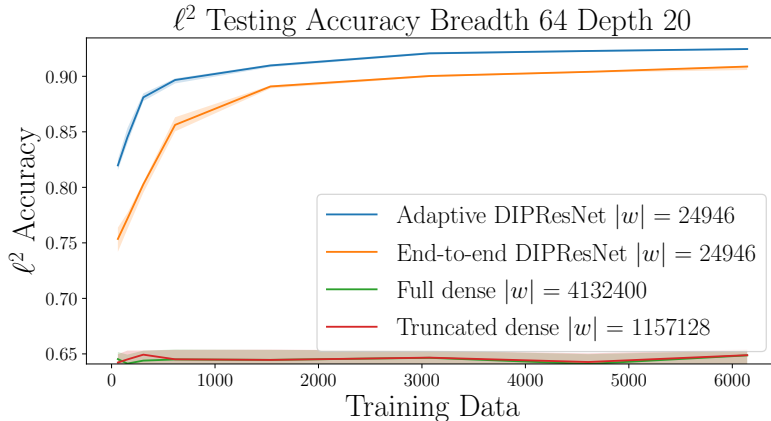


Fig. 11: Depth 20 Breadth 64 Comparison of Networks

5. Summary and Conclusion. In this work, we propose an adaptive projected ResNet surrogate strategy for learning high dimensional parametric maps from limited training data. This type of surrogate can achieve high accuracy for limited training data, and can help make possible the accurate solution of high dimensional outer-loop problems on a limited number of queries from an expensive high fidelity direct numerical simulation.

Many high dimensional parametric mappings admit low dimensional structure due to physics, sparse observations of field quantities, geometry of data, concentration of measure, or other mathematical structure. This inspires the highly scalable surrogate strategy: parametrization of the full map between map-informed reduced basis of both the inputs and outputs [4, 38]. In this work we motivate both theoretically and algorithmically, an architectural strategy for learning the reduced nonlinear mapping via adaptively trained projected ResNets. We begin by proving a universal approximation property of this class of functions. Error bounds that we derive are based on theory for input-output reduced ridge function approximations of high dimensional parametric mappings, and recent theory establishing a connection between ResNets and control flow function approximations [21]. This theoretical construction of the approximation capabilities of ResNets motivates our adaptive algorithm for the construction of these surrogates.

Two numerical results demonstrate the efficacy of these adaptively trained projected ResNet, one from aerodynamic shape optimization, and another from parametric PDE inference. These results show that these projected ResNet can achieve superior generalization accuracy to other conventional deep learning methods, all while having much smaller weight dimensional spaces. Additionally numerical results demonstrate that the performance of the adaptively constructed ResNets uniformly outperformed the same exact architecture trained end-to-end; showing the upside of merging the construction and optimizing processes, as the theory suggests.

Conventional wisdom in machine learning suggests that the best strategies for reconstructing input-output mappings is to build overparametrized neural networks which have much larger weight dimensions than the available training data cardinality. In this case the associated large configuration spaces give the optimizer more leeway to fit the data. The typical setting for machine learning however is “big-data”, where large training datasets are available for the empirical risk minimization problem (or the model is already initialized well, e.g. transfer learning). In the setting that we are concerned with, the opposite seems to hold, that when one is left with few samples of a very high dimensional map, it can be a liability to overparametrize.

A last upside worth noting is the computational economy of our proposed approach. Improving the computational economy of neural networks, (e.g. “pruning” [5]) is an issue of recent concern. In order to scale machine learning models to energy and memory constrained environments parsimonious network surrogates are needed. This approaches attempts to build an already “pruned” model from scratch.

Appendix A. Proof of Theorem 2.2.

Let $\epsilon > 0$ be arbitrary, and let χ_K denote the characteristic function for the compact set $K \subset \mathbb{R}^{d_M}$, and $K_r \subset \mathbb{R}^r$ be the restriction of K to the reduced basis $V_r \in \mathbb{R}^{d_M \times r}$, i.e. $K_r = \{V_r^T m | m \in K\}$. Note that since we are in finite dimensions we can work with probability densities for $\nu(m)$, which we refer to as $\pi(m)$.

Note that since $q \in L^2(\mathbb{R}^{d_M}, \nu; \mathbb{R}^{d_Q})$, the ridge function approximation $\Phi_r q_r$ is as well if $\zeta_r < \infty$. Since $\|\Phi\|_{\ell^2(\mathbb{R}^{d_Q \times r})} = 1$, q_r is $L^2(\mathbb{R}^{d_M}, \nu; \mathbb{R}^r)$, and can be arbitrarily well approximated by a continuous function $q_r^{\text{cont}} \in C^1(\mathbb{R}^r)$ when restricted to K , since continuous functions are dense in L^2 . Let q_r^{cont} be such that $\mathbb{E}_\nu[\|q_r - q_r^{\text{cont}}\|_{\ell^2(\mathbb{R}^r)} \chi_{K_r}] < \frac{\epsilon}{3}$.

Proposition 4.11 in [21] states that any continuous function $q_r^{\text{cont}} \in C(\mathbb{R}^r)$ can be approximated arbitrarily well by a finite time control flow representation so long as the set of right hand sides \mathcal{F} for the control flow is closed under affine operations, and the closure of this set under the topology of compact convergence contains a well-function. The restricted affine invariance requires that if $f \in \mathcal{F}$, then $Df(A \cdot + b)$ is also in \mathcal{F} , for D, A diagonal matrices in $\mathbb{R}^{r \times r}$ with diagonal entries $d_i = \pm 1$ and $a_i \leq 1$, and $b \in \mathbb{R}^r$ arbitrary. We note that the family of right hand sides associated with the continuous analogue of ResNet satisfies this property. The well-function property requires that the activation function used in the ResNet can be used to build a function that is arbitrarily close to zero when restricted to an open bounded set (e.g. ReLU, sigmoid, tanh etc.). For a lengthier discussion of these requirements see section 2 in [21]. Proposition 4.11 along with these properties allows that there exists a finite time $T < \infty$ control flow mapping of the form:

$$(A.1a) \quad \frac{dz}{dt} = w_1(t)\sigma(w_0(t) + b(t))$$

$$(A.1b) \quad z(0) = V_r^T m$$

$$(A.1c) \quad \xi_T(m) = z(T; m)$$

such that $\int_{K_r} \|\xi_T - q_r^{\text{cont}}\|_{\ell^2(\mathbb{R}^r)} dm < \frac{\epsilon}{3}$. Note that the mapping is effectively $z : (0, T] \times \mathbb{R}^r \rightarrow \mathbb{R}^r$, but is parametrized over \mathbb{R}^{d_M} via $V_r^T m$. We can extend this result to integration with respect to the probability density function ν by noting that by

Cauchy Schwarz,

$$(A.2) \quad \int_K \|\xi_T - q_r^{\text{cont}}\|_{\ell^2(\mathbb{R}^r)} d\nu(m) = \int_K \|\xi_T - q_r^{\text{cont}}\|_{\ell^2(\mathbb{R}^r)} \pi(m) dm \leq \int_K \|\xi_T - q_r^{\text{cont}}\|_{\ell^2(\mathbb{R}^r)} dm.$$

The system (A.1) can be approximated to arbitrary precision via an Explicit Euler discretization with time discretization Δt which yields the ResNet:

$$(A.3) \quad z_{k+1} = z_k + \Delta t w_{1k} \sigma(w_{0k} z_k + b_k)$$

Assuming the right hand side of (A.1a) is Lipschitz with bound L_{ResNet} , and the true solution $z(t; m)$ to (A.1) is itself twice differentiable for all $t \in (0, T)$, and for all $m \in K$ we have that $\max_{t \in (0, T)} \left\| \frac{\partial^2 z}{\partial t^2} \right\|_{\ell^2(\mathbb{R}^r)} \leq M$, then the global truncation error for the Explicit Euler approximation can be bounded by

$$(A.4) \quad \int_K \|\xi_T^{E.E.}(m) - \xi_T(m)\|_{\ell^2(\mathbb{R}^r)} d\nu(m) \leq \frac{e^{L_{\text{ResNet}} T} - 1}{2L_{\text{ResNet}}} M \Delta t |K| \leq \frac{\epsilon}{3},$$

see [40]. The requirements for Δt become:

$$(A.5) \quad \Delta t \leq \frac{2}{3} \frac{\epsilon L_{\text{ResNet}}}{M |K| (e^{L_{\text{ResNet}} T} - 1)},$$

for homogenous time steps we have $\Delta t = \frac{T}{\text{depth}}$, which gives us the following bound:

$$(A.6) \quad \text{depth} \geq \frac{3}{2} \frac{M |K| T (e^{L_{\text{ResNet}} T} - 1)}{\epsilon L_{\text{ResNet}}}$$

Combining all of these results together we can bound as follows:

$$(A.7) \quad \begin{aligned} \mathbb{E}_\nu [\|\xi_T^{E.E.} - q_r\|_{\ell^2(\mathbb{R}^r)}] &\leq \\ \mathbb{E}_\nu [\|\xi_T^{E.E.} - \xi_T\|_{\ell^2(\mathbb{R}^r)} + \|\xi_T - q_r^{\text{cont}}\|_{\ell^2(\mathbb{R}^r)} + \|q_r^{\text{cont}} - q_r\|_{\ell^2(\mathbb{R}^r)}] &\leq \\ \frac{\epsilon}{3} + \frac{\epsilon}{3} + \frac{\epsilon}{3} \end{aligned}$$

The final result comes from setting $\epsilon = \zeta_r$ (since it was arbitrary), and then noting that $\xi_T^{E.E.}(m, w) = f_r(m, w)$,

$$(A.8) \quad \begin{aligned} \int_K \|q(m) - \widehat{\Phi}_r f_r(V_r^T m, w)\|_{\ell^2(\mathbb{R}^{d_Q})} d\nu(m) &\leq \\ \int_K \|q(m) - \widehat{\Phi}_r q_r(V_r^T m, w)\|_{\ell^2(\mathbb{R}^{d_Q})} + \|\widehat{\Phi}_r(q_r(V_r^T m) - f_r(V_r^T m, w))\|_{\ell^2(\mathbb{R}^{d_Q})} d\nu(m) \end{aligned}$$

and

$$(A.9) \quad \begin{aligned} \|\widehat{\Phi}_r(q_r(V_r^T m) - f_r(V_r^T m, w))\|_{\ell^2(\mathbb{R}^{d_Q})} &\leq \\ \|\widehat{\Phi}_r\|_{\ell^2(\mathbb{R}^{d_Q \times r})} \|q_r(V_r^T m) - f_r(V_r^T m, w)\|_{\ell^2(\mathbb{R}^r)} &\leq \\ \|q_r(V_r^T m) - f_r(V_r^T m, w)\|_{\ell^2(\mathbb{R}^r)} \end{aligned}$$

since $\widehat{\Phi}_r$ is orthonormal.

Note additionally that the e^T complexity in the depth comes only from the global truncation error for Explicit Euler, which is a conservative bound. In [21] the control flows they construct are actually piecewise constant in time, which is sufficient since simple functions are dense in continuous functions. In that case Explicit Euler is an exact time integrator, and then the the depth complexity can be reduced to $O\left(\frac{T|K|}{\epsilon}\right)$. The bound we give above, however, is more general since it represents discretizations of continuous time control flows.

Appendix B. Numerical Results Appendix.

B.1. MACH-Aero Design Framework. MACH design framework aims at Multidisciplinary design optimization of Aircraft Configurations with High fidelity while MACH-Aero² implements MACH on aerodynamic design optimization. Aerodynamic design by MACH-Aero sets up an optimization problem using the `python` interface `pyOptSparse` [46] and starts with an initial design q_0 under specified design requirements m , and uses gradient information to find the optimum airfoil design (control points and angle of attack). The steps are as follows. (1) A baseline design volume mesh is generated using `pyHyp` [43], which will be deformed for any given value of design variables. (2) The SNOPT (Sparse Nonlinear OPTimizer) [14] updates design variables and sends the new design to the geometry parameterization. (3) The geometry parameterization module (`pyGeo`) [19] performs the geometry deformation, and computes the values of geometric constraints and corresponding gradients. (4) The volume mesh deformation module generates the deformed mesh based on the deformed geometry. (5) The CFD module (`ADflow` [26] or `DAFoam` [15]) computes high fidelity forward and adjoint flow fields on the deformed mesh, and sends the objective function and constraint values and computed gradient information back to the optimizer. The process is iterated until an optimal design $q(m)$ is found that satisfies the optimality and feasibility conditions.

B.2. Aerodynamic Dataset Split. Latin hypercube sampling (LHS) [29], as an advanced version of Monte Carlo sampling strategy, has been widely used in various engineering fields. In this work, we generate the original data set using LHS, infill more samples using augmented LHS (`augLHS`) [44], and extract subsets from the whole data set using conditioned LHS (`cLHS`) [30].

Instead of completely generating random samples, LHS divides the space of $[0, 1]^M$ into evenly distribution N sub-intervals in each dimension, where M is the dimension of a design-variable space and N is the number of samples to be generated. Taking $M = 2$ as an example, the division makes a $N \times N$ matrix. LHS sweeps through the columns searching for empty rows among which LHS selects a random one to generate a value (within the sub-interval) for each column. The generated values are used as cumulative distribution function (CDF) values of corresponding pre-assigned probabilistic distributions, such as uniform and Gaussian distributions. The inverse CDF values are the sampled parameters.

Infill sampling using `augLHS` enlarges a small dataset while maintaining the characteristics of LHS. In particular, `augLHS` follows the similar sweeping principle as LHS except that `augLHS` divides the original design-variable space into a $(N + N_{new}) \times N + N_{new}$ matrix where N_{new} is the number of new samples to be added into the small dataset. The following steps are the same as LHS. Extract-

²<https://github.com/mdolab/MACH-Aero>

ing data samples while maintaining LHS characteristics plays an important role in comparing various neural network surrogates on extracted small datasets. We see cLHS as an inverse process of augLHS by dividing the original design-variable space into a $N_{sub} \times N_{sub}$ matrix where N_{sub} is the number of samples to be extracted and $N_{sub} < N$. In this work, we use the built-in functions for LHS, augLHS, and cLHS methods within the R programming language [18]. For the purpose of reproducibility, we set the random seeds for LHS and augLHS as an arbitrary number, 42. We set the cLHS random seeds to be the 50 integers within $[0, 49]$ to extract small data sets to compare neural network surrogate approaches. Specifically, we generated 500 LHS data samples and infill 500 more samples using augLHS, then let cLHS address the data extraction.

B.3. Two Step Optimization. We use an Adam optimizer with default settings for a small number of epochs for each adaptive layer training (total epochs sums to 50), and then perform one final end-to-end training with LRSFN [36] for 50 “epoch equivalent” neural network sweeps (i.e. forward and backward pass). In this case we allow all intermediate ResNet layers (and the output layer) to be trained at each adaptive step, so Adam has “converged” in this process. Below we compare the results of performing this last training with Adam, and with LRSFN using Hessian rank $r = 40$. We used gradient batch size of 2 for Adam, and gradient batch size of 4 and Hessian batch size of 2 for LRSFN. Both optimizers use $\alpha = 1e - 3$ fixed step sizes. Some results are shown below and they are consistently representative of the pattern seen.

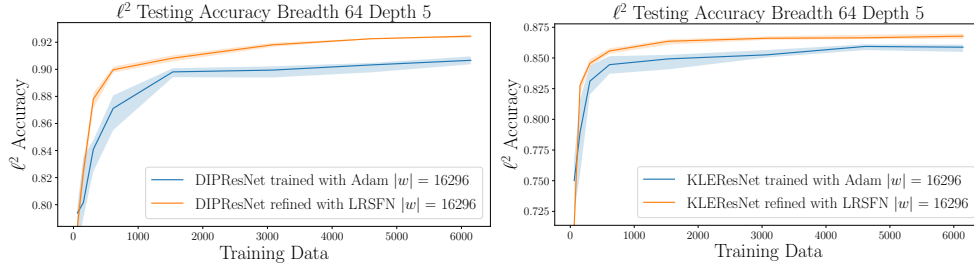


Fig. 12: Depth 5 Breadth 32 Optimizer Comparison

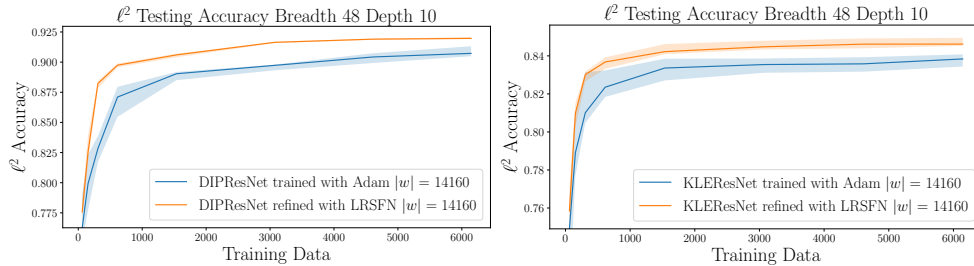


Fig. 13: Depth 10 Breadth 48 Optimizer Comparison

REFERENCES

- [1] M. ABADI, P. BARHAM, J. CHEN, Z. CHEN, A. DAVIS, J. DEAN, M. DEVIN, S. GHEMAWAT, G. IRVING, M. ISARD, ET AL., *Tensorflow: A system for large-scale machine learning*, in 12th {USENIX} symposium on operating systems design and implementation ({OSDI} 16), 2016, pp. 265–283.
- [2] M. S. ALNÆS, J. BLECHTA, J. HAKE, A. JOHANSSON, B. KEHLET, A. LOGG, C. RICHARDSON, J. RING, M. E. ROGNES, AND G. N. WELLS, *The fenics project version 1.5*, Archive of Numerical Software, 3 (2015), <https://doi.org/10.11588/ans.2015.100.20553>.
- [3] A. G. BAYDIN, B. A. PEARLMUTTER, A. A. RADUL, AND J. M. SISKIND, *Automatic differentiation in machine learning: a survey*, Journal of machine learning research, 18 (2018).
- [4] K. BHATTACHARYA, B. HOSSEINI, N. B. KOVACHKI, AND A. M. STUART, *Model reduction and neural networks for parametric pdes*, arXiv preprint arXiv:2005.03180, (2020).
- [5] D. BLALOCK, J. J. G. ORTIZ, J. FRANKLE, AND J. GUTTAG, *What is the state of neural network pruning?*, arXiv preprint arXiv:2003.03033, (2020).
- [6] K. BOLLINGER AND H. SCHAEFFER, *Reduced order modeling using shallow relu networks with grassmann layers*, arXiv preprint arXiv:2012.09940, (2020).
- [7] K. H. R. CHAN, Y. YU, C. YOU, H. QI, J. WRIGHT, AND Y. MA, *Redunet: A white-box deep network from the principle of maximizing rate reduction*, arXiv preprint arXiv:2105.10446, (2021).
- [8] R. T. CHEN, Y. RUBANOVA, J. BETTENCOURT, AND D. DUVENAUD, *Neural ordinary differential equations*, arXiv preprint arXiv:1806.07366, (2018).
- [9] W. CHEW AND Q. LIU, *Perfectly matched layers for elastodynamics: a new absorbing boundary condition*, Journal of Computational Acoustics, 4 (1996), pp. 341–359.
- [10] G. CYBENKO, *Approximation by superpositions of a sigmoidal function*, Mathematics of control, signals and systems, 2 (1989), pp. 303–314.
- [11] C. DONG, L. LIU, Z. LI, AND J. SHANG, *Towards adaptive residual network training: A neural-ode perspective*, in International conference on machine learning, PMLR, 2020, pp. 2616–2626.
- [12] W. E, C. MA, AND L. WU, *Barron spaces and the compositional function spaces for neural network models*, arXiv preprint arXiv:1906.08039, (2019).
- [13] S. FRESCA AND A. MANZONI, *Pod-dl-rom: enhancing deep learning-based reduced order models for nonlinear parametrized pdes by proper orthogonal decomposition*, Computer Methods in Applied Mechanics and Engineering, 388 (2022), p. 114181.
- [14] P. E. GILL, W. MURRAY, AND M. A. SAUNDERS, *SNOPT: An SQP algorithm for large-scale constrained optimization*, SIAM Journal of Optimization, 12 (2002), pp. 979–1006, <https://doi.org/10.1137/S1052623499350013>.
- [15] P. HE, C. A. MADER, J. R. R. A. MARTINS, AND K. J. MAKI, *DAFoam: An open-source adjoint framework for multidisciplinary design optimization with OpenFOAM*, AIAA Journal, 58 (2020), <https://doi.org/10.2514/1.J058853>.
- [16] K. HORNIK, *Approximation capabilities of multilayer feedforward networks*, Neural networks, 4 (1991), pp. 251–257.
- [17] G. HUGHES, *On the mean accuracy of statistical pattern recognizers*, IEEE transactions on information theory, 14 (1968), pp. 55–63.
- [18] R. IHAKA, *R : Past and future history*, Technical Report, (1998), <https://doi.org/10.1.1.331.299>.
- [19] G. K. W. KENWAY, G. J. KENNEDY, AND J. R. R. A. MARTINS, *A CAD-free approach to high-fidelity aerostructural optimization*, in Proceedings of the 13th AIAA/ISSMO Multidisciplinary Analysis Optimization Conference, Fort Worth, TX, September 2010. AIAA 2010-9231.
- [20] N. KOVACHKI, Z. LI, B. LIU, K. AZIZZADENESHELI, K. BHATTACHARYA, A. STUART, AND A. ANANDKUMAR, *Neural operator: Learning maps between function spaces*, arXiv preprint arXiv:2108.08481, (2021).
- [21] Q. LI, T. LIN, AND Z. SHEN, *Deep learning via dynamical systems: An approximation perspective*, arXiv preprint arXiv:1912.10382, (2019).
- [22] Z. LI, N. KOVACHKI, K. AZIZZADENESHELI, B. LIU, K. BHATTACHARYA, A. STUART, AND A. ANANDKUMAR, *Neural operator: Graph kernel network for partial differential equations*, arXiv preprint arXiv:2003.03485, (2020).
- [23] H. LIN AND S. JEGELKA, *Resnet with one-neuron hidden layers is a universal approximator*, arXiv preprint arXiv:1806.10909, (2018).
- [24] L. LU, P. JIN, AND G. E. KARNIAKAKIS, *Deeponet: Learning nonlinear operators for identifying differential equations based on the universal approximation theorem of operators*, arXiv preprint arXiv:1910.03193, (2019).
- [25] Z. LU, H. PU, F. WANG, Z. HU, AND L. WANG, *The expressive power of neural networks: A view from the width*, in Proceedings of the 31st International Conference on Neural

- Information Processing Systems, 2017, pp. 6232–6240.
- [26] C. A. MADER, G. K. W. KENWAY, A. YILDIRIM, AND J. R. R. A. MARTINS, *ADflow—an open-source computational fluid dynamics solver for aerodynamic and multidisciplinary optimization*, Journal of Aerospace Information Systems, (2020), <https://doi.org/10.2514/1.1010796>.
 - [27] A. MANZONI, F. NEGRI, AND A. QUARTERONI, *Dimensionality reduction of parameter-dependent problems through proper orthogonal decomposition*, Annals of Mathematical Sciences and Applications, 1 (2016), pp. 341–377.
 - [28] P.-G. MARTINSSON AND J. A. TROPP, *Randomized numerical linear algebra: Foundations and algorithms*, Acta Numerica, 29 (2020), pp. 403–572.
 - [29] M. D. MCKAY, R. J. BECKMAN, AND W. J. CONOVER, *A comparison of three methods for selecting values of input variables in the analysis of output from a computer code*, Technometrics, 21 (1979), pp. 239–245.
 - [30] B. MINASNY AND A. MCBRATNEY, *A conditioned latin hypercube method for sampling in the presence of ancillary information*, Computers & Geosciences, 32 (2006), pp. 1378–1388, <https://doi.org/10.1016/j.cageo.2005.12.009>.
 - [31] N. H. NELSEN AND A. M. STUART, *The random feature model for input-output maps between banach spaces*, arXiv preprint arXiv:2005.10224, (2020).
 - [32] H. V. NGUYEN AND T. BUI-THANH, *Model-constrained deep learning approaches for inverse problems*, arXiv preprint arXiv:2105.12033, (2021).
 - [33] T. O’LEARY-ROSEBERRY, *Efficient and dimension independent methods for neural network surrogate construction and training*, PhD thesis, 2020.
 - [34] T. O’LEARY-ROSEBERRY, *hessianlearn: Stochastic Nonconvex Optimization in TensorFlow and keras*, 2021, <https://doi.org/10.5281/zenodo.4608644>, <https://github.com/tomoleary/hessianlearn>.
 - [35] T. O’LEARY-ROSEBERRY, N. ALGER, AND O. GHATTAS, *Inexact Newton methods for stochastic nonconvex optimization with applications to neural network training*, arXiv preprint arXiv:1905.06738, (2019).
 - [36] T. O’LEARY-ROSEBERRY, N. ALGER, AND O. GHATTAS, *Low rank saddle free Newton: A scalable method for stochastic nonconvex optimization*, arXiv preprint arXiv:2002.02881, (2020).
 - [37] T. O’LEARY-ROSEBERRY AND U. VILLA, *hippyflow: Dimension reduced surrogate construction for parametric PDE maps in Python*, 2021, <https://doi.org/10.5281/zenodo.4608729>, <https://github.com/hippylib/hippyflow>.
 - [38] T. O’LEARY-ROSEBERRY, U. VILLA, P. CHEN, AND O. GHATTAS, *Derivative-informed projected neural networks for high-dimensional parametric maps governed by pdes*, Computer Methods in Applied Mechanics and Engineering, 388 (2022), p. 114199.
 - [39] A. QUARTERONI, A. MANZONI, AND F. NEGRI, *Reduced basis methods for partial differential equations: an introduction*, vol. 92, Springer, 2015.
 - [40] A. QUARTERONI, R. SACCO, AND F. SALERI, *Numerical mathematics*, vol. 37, Springer Science & Business Media, 2010.
 - [41] L. RUTHOTTO AND E. HABER, *Deep neural networks motivated by partial differential equations*, Journal of Mathematical Imaging and Vision, 62 (2020), pp. 352–364.
 - [42] C. SCHWAB AND R. A. TODOR, *Karhunen–Loève approximation of random fields by generalized fast multipole methods*, Journal of Computational Physics, 217 (2006), pp. 100–122.
 - [43] N. SECCO, G. K. W. KENWAY, P. HE, C. A. MADER, AND J. R. R. A. MARTINS, *Efficient mesh generation and deformation for aerodynamic shape optimization*, AIAA Journal, (2021), <https://doi.org/10.2514/1.1059491>.
 - [44] M. STEIN, *Large sample properties of simulations using latin hypercube sampling*, Technometrics, 29 (1987), pp. 143–151, <https://doi.org/10.1080/00401706.1987.10488205>.
 - [45] U. VILLA, N. PETRA, AND O. GHATTAS, *hIPPYlib: An Extensible Software Framework for Large-Scale Inverse Problems Governed by PDEs; Part I: Deterministic Inversion and Linearized Bayesian Inference*, Transactions on Mathematical Software, in print (2020), <https://arxiv.org/abs/1909.03948>.
 - [46] N. WU, G. KENWAY, C. A. MADER, J. JASA, AND J. R. R. A. MARTINS, *pyoptspare: A python framework for large-scale constrained nonlinear optimization of sparse systems*, Journal of Open Source Software, 5 (2020), p. 2564, <https://doi.org/10.21105/joss.02564>.
 - [47] A. YAGUCHI, T. SUZUKI, S. NITTA, Y. SAKATA, AND A. TANIZAWA, *Scalable deep neural networks via low-rank matrix factorization*, (2019).
 - [48] O. ZAHM, P. G. CONSTANTINE, C. PRIEUR, AND Y. M. MARZOUK, *Gradient-based dimension reduction of multivariate vector-valued functions*, SIAM Journal on Scientific Computing, 42 (2020), pp. A534–A558.